Electronic supporting information for:

A diamagnetic iron(III) complex and its twisted sister – Structural evidence on partial spin state change in a crystalline iron complex

Esko Salojärvi,[a] Anssi Peuronen,[ab] Akseli Mansikkamäki,[e] Jani Moilanen,[b] Hannu Huhtinen,[c] Johan Linden,[d] Mika Lastusaari[a] and Ari Lehtonen[a*]

[a]Inorganic Materials Chemistry research group, Department of Chemistry, University of Turku, FI-20014 Turku, Finland

[b]Department of Chemistry, P.O. Box 35, University of Jyväskylä, FI-40014 Jyväskylä, Finland

[c]Wihuri Physical Laboratory, Department of Physics and Astronomy, University of Turku, FI-20014 Turku, Finland

[d]Department of Physics, Åbo Akademi University FI-20500, Turku/Åbo, Finland

[e]NMR Research Unit, University of Oulu, P. O. Box 3000, 90014 Oulu, Finland

Content:

Table S1. Summary of crystallographic data for **1** and **2**.

	1	**2** at 120 K	**2** at 95 K
Empirical formula	$C_{68}H_{90}FeN_4O_4$	$C_{68}H_{86}FeN_4O_4$	$C_{68}H_{86}FeN_4O_4$
Formula weight	1083.28	1079.25	1079.25
Temperature/K	120.0(1)	120.0(1)	95.0(1)
Crystal system	Triclinic	Monoclinic	Monoclinic
Space group	*P*-1	$P2_1/n$	$P2_1/c$
a/Å	15.0168(4)	20.6261(9)	33.0889(5)
b/Å	15.4772(6)	26.6719(9)	26.8096(3)
c/Å	16.4464(4)	23.2777(9)	28.7832(4)
α/°	94.107(2)	90	90
β/°	107.195(2)	97.960(4)	96.7035(12)
γ/°	115.663(3)	90	90
Volume/Å^3	3201.69(19)	12682.5(9)	25359.0(6)
Z	2	8	16
ρ_{calc} g cm^{-3}	1.124	1.13	1.131
μ/mm^{-1}	2.254	2.276	2.276
F(000)	1168	4640	9280
Crystal size/mm^3	0.241 × 0.099 × 0.061	0.147 × 0.072 × 0.043	0.371 × 0.071 × 0.056
Radiation	Cu Kα (λ = 1.54184)	Cu Kα (λ = 1.54184)	Cu Kα (λ = 1.54184)
2Θ range for data collection/°	5.782 to 153.368	7.658 to 139.998	4.254 to 139.998
Index ranges	-18 ≤ h ≤ 13, -19 ≤ k ≤ 18, -20 ≤ l ≤ 20	-25 ≤ h ≤ 25, -23 ≤ k ≤ 32, -28 ≤ l ≤ 22	-40 ≤ h ≤ 39, -32 ≤ k ≤ 22, -35 ≤ l ≤ 29
Reflections collected	25813	41536	102261
Independent reflections	13175 [R_{int} = 0.0264, R_{sigma} = 0.0364]	23680 [R_{int} = 0.0846, R_{sigma} = 0.1331]	47984 [R_{int} = 0.0731, R_{sigma} = 0.1010]
Data/restraints/ parameters	13175/0/726	23680/15/1433	47984/36/2904
Goodness-of-fit on F^2	1.032	1.034	0.983
Final R indexes [I>=2σ (I)]	R_1 = 0.0405, wR_2 = 0.1027	R_1 = 0.0818, wR_2 = 0.1717	R_1 = 0.0546, wR_2 = 0.1086
Final R indexes [all data]	R_1 = 0.0489, wR_2 = 0.1086	R_1 = 0.1488, wR_2 = 0.2052	R_1 = 0.1069, wR_2 = 0.1303
Largest diff. peak/hole / e Å^{-3}	0.55/-0.33	0.88/-0.42	0.59/-0.35

Table S2. Selected bond lengths (Å) for **1**.

Fe1	O1	1.9470(12)
Fe1	O3	1.9579(11)
Fe1	N1	1.8760(13)
Fe1	N2	1.9692(14)
Fe1	N3	1.8744(13)
Fe1	N4	1.9616(13)
O1	C8	1.3247(19)
O2	C14	1.3620(19)
O3	C42	1.3342(19)
O4	C48	1.363(2)
N1	C1	1.349(2)
N1	C7	1.388(2)
N2	C6	1.326(2)
N2	C13	1.424(2)
N3	C35	1.345(2)
N3	C41	1.392(2)
N4	C40	1.336(2)
N4	C47	1.4247(19)
C1	C2	1.421(2)
C1	C6	1.451(2)
C2	C3	1.365(2)
C3	C4	1.420(3)
C4	C5	1.356(2)
C5	C6	1.431(2)
C7	C8	1.423(2)
C7	C12	1.403(2)
C8	C9	1.423(2)
C9	C10	1.386(2)
C9	C19	1.534(2)
C10	C11	1.416(2)
C11	C12	1.377(2)
C11	C23	1.531(2)
C13	C14	1.395(2)
C13	C18	1.398(2)
C14	C15	1.404(2)
C15	C16	1.392(2)
C15	C27	1.538(2)
C16	C17	1.396(2)
C17	C18	1.385(2)

Table S3. Selected bond lengths (Å) for **2** determined at 120 K.

Fe1A	O1A	1.998(3)	Fe1B	O1B	2.000(3)
Fe1A	O3A	2.013(3)	Fe1B	O3B	1.997(4)
Fe1A	N1A	2.079(4)	Fe1B	N1B	2.083(4)
Fe1A	N2A	2.133(4)	Fe1B	N2B	2.123(4)
Fe1A	N3A	2.075(4)	Fe1B	N3B	2.046(4)
Fe1A	N4A	2.145(4)	Fe1B	N4B	2.144(4)
O1A	C8A	1.306(6)	O1B	C8B	1.294(6)
O2A	C5A	1.381(6)	O2B	C5B	1.380(6)
O2A	C14A	1.397(6)	O2B	C14B	1.378(6)
O3A	C42A	1.316(6)	O3B	C42B	1.307(6)
O4A	C39A	1.367(6)	O4B	C39B	1.366(7)
O4A	C48A	1.384(5)	O4B	C48B	1.366(6)
N1A	C1A	1.354(6)	N1B	C1B	1.361(6)
N1A	C7A	1.372(6)	N1B	C7B	1.362(6)
N2A	C6A	1.332(6)	N2B	C6B	1.333(6)
N2A	C13A	1.389(6)	N2B	C13B	1.384(6)
N3A	C35A	1.351(6)	N3B	C35B	1.336(7)
N3A	C41A	1.373(6)	N3B	C41B	1.382(6)
N4A	C40A	1.336(6)	N4B	C40B	1.333(6)
N4A	C47A	1.390(6)	N4B	C47B	1.398(6)
C1A	C2A	1.410(6)	C1B	C2B	1.423(7)
C1A	C6A	1.457(6)	C1B	C6B	1.448(7)
C2A	C3A	1.366(7)	C2B	C3B	1.361(8)
C3A	C4A	1.424(7)	C3B	C4B	1.419(9)
C4A	C5A	1.341(7)	C4B	C5B	1.347(8)
C5A	C6A	1.414(7)	C5B	C6B	1.423(7)
C7A	C8A	1.433(6)	C7B	C8B	1.443(6)
C7A	C12A	1.412(6)	C7B	C12B	1.415(6)
C8A	C9A	1.422(7)	C8B	C9B	1.432(6)
C9A	C10A	1.372(7)	C9B	C10B	1.380(7)
C9A	C19A	1.536(7)	C9B	C19B	1.528(6)
C10A	C11A	1.417(7)	C10B	C11B	1.414(7)
C11A	C12A	1.375(7)	C11B	C12B	1.361(7)
C11A	C23A	1.537(7)	C11B	C23B	1.535(6)
C13A	C14A	1.398(7)	C13B	C14B	1.411(7)
C13A	C18A	1.392(7)	C13B	C18B	1.393(7)
C14A	C15A	1.404(7)	C14B	C15B	1.398(7)
C15A	C16A	1.379(7)	C15B	C16B	1.381(7)
C15A	C27A	1.539(7)	C15B	C27B	1.534(7)
C16A	C17A	1.390(7)	C16B	C17B	1.415(7)
C17A	C18A	1.379(7)	C17B	C18B	1.379(6)

Table S4. Selected bond lengths (Å) for **2** determined at 95 K.

Fe1A	O1A	1.9971(18)	Fe1C	O1C	2.0014(18)
Fe1A	O3A	2.0125(19)	Fe1C	O3C	2.0196(19)
Fe1A	N1A	2.072(2)	Fe1C	N1C	2.076(2)
Fe1A	N2A	2.126(2)	Fe1C	N2C	2.128(2)
Fe1A	N3A	2.078(2)	Fe1C	N3C	2.085(2)
Fe1A	N4A	2.146(2)	Fe1C	N4C	2.157(2)
O1A	C8A	1.303(3)	O1C	C1C	1.305(3)
O2A	C5A	1.368(3)	O2C	C11C	1.374(3)
O2A	C14A	1.386(4)	O2C	C14C	1.382(3)
O3A	C41A	1.303(3)	O3C	C41C	1.308(3)
O4A	C39A	1.371(3)	O4C	C39C	1.375(3)
O4A	C48A	1.389(3)	O4C	C48C	1.382(3)
N1A	C1A	1.349(4)	N1C	C6C	1.370(4)
N1A	C7A	1.365(4)	N1C	C7C	1.350(4)
N2A	C6A	1.336(4)	N2C	C12C	1.333(4)
N2A	C13A	1.394(3)	N2C	C13C	1.391(4)
N3A	C35A	1.344(4)	N3C	C35C	1.347(4)
N3A	C46A	1.367(4)	N3C	C46C	1.362(4)
N4A	C40A	1.335(4)	N4C	C40C	1.337(4)
N4A	C47A	1.381(4)	N4C	C47C	1.383(4)
C1A	C2A	1.415(4)	C1C	C2C	1.430(4)
C1A	C6A	1.455(4)	C1C	C6C	1.438(4)
C2A	C3A	1.366(4)	C2C	C3C	1.379(4)
C3A	C4A	1.423(4)	C2C	C19C	1.534(4)
C4A	C5A	1.360(4)	C3C	C4C	1.418(5)
C5A	C6A	1.424(4)	C4C	C5C	1.377(4)
C7A	C8A	1.445(4)	C4C	C23C	1.535(4)
C7A	C12A	1.417(4)	C5C	C6C	1.410(4)
C8A	C9A	1.432(4)	C7C	C8C	1.420(4)
C9A	C10A	1.383(4)	C7C	C12C	1.457(4)
C9A	C19A	1.529(4)	C8C	C9C	1.378(4)
C10A	C11A	1.414(4)	C9C	C10C	1.410(4)
C11A	C12A	1.373(4)	C10C	C11C	1.367(4)
C11A	C23A	1.538(4)	C11C	C12C	1.417(4)
C13A	C14A	1.400(4)	C13C	C14C	1.407(4)
C13A	C18A	1.400(4)	C13C	C18C	1.397(4)
C14A	C15A	1.405(4)	C14C	C15C	1.399(4)
C15A	C16A	1.392(5)	C15C	C16C	1.393(4)
C15A	C27A	1.535(4)	C15C	C27C	1.532(4)
C16A	C17A	1.395(5)	C16C	C17C	1.407(4)
C17A	C18A	1.385(4)	C17C	C18C	1.380(4)

Fe1B	O1B	2.010(2)	Fe1D	O1D	1.9613(19)
Fe1B	O3B	2.0075(19)	Fe1D	O3D	1.9555(19)
Fe1B	N1B	2.064(2)	Fe1D	N1D	1.903(2)
Fe1B	N2B	2.141(2)	Fe1D	N2D	1.987(2)
Fe1B	N3B	2.093(2)	Fe1D	N3D	1.924(2)
Fe1B	N4B	2.136(2)	Fe1D	N4D	1.979(2)
O1B	C7B	1.306(4)	O1D	C7D	1.308(4)
O2B	C5B	1.372(4)	O2D	C5D	1.372(4)
O2B	C14B	1.381(4)	O2D	C14D	1.383(4)
O3B	C41B	1.296(3)	O3D	C41D	1.308(3)
O4B	C39B	1.373(4)	O4D	C39D	1.363(4)
O4B	C48B	1.381(3)	O4D	C48D	1.377(4)
N1B	C1B	1.344(4)	N1D	C1D	1.345(4)
N1B	C12B	1.369(4)	N1D	C12D	1.391(4)
N2B	C6B	1.340(4)	N2D	C6D	1.338(4)
N2B	C13B	1.394(4)	N2D	C13D	1.402(4)
N3B	C35B	1.348(4)	N3D	C35D	1.360(4)
N3B	C46B	1.363(4)	N3D	C46D	1.379(4)
N4B	C40B	1.335(4)	N4D	C40D	1.334(4)
N4B	C47B	1.392(4)	N4D	C47D	1.400(4)
C1B	C2B	1.415(4)	C1D	C2D	1.431(4)
C1B	C6B	1.452(4)	C1D	C6D	1.436(4)
C2B	C3B	1.368(5)	C2D	C3D	1.357(5)
C3B	C4B	1.416(5)	C3D	C4D	1.419(5)
C4B	C5B	1.359(5)	C4D	C5D	1.357(4)
C5B	C6B	1.420(4)	C5D	C6D	1.413(4)
C7B	C8B	1.438(4)	C7D	C8D	1.434(4)
C7B	C12B	1.434(4)	C7D	C12D	1.423(4)
C8B	C9B	1.385(5)	C8D	C9D	1.379(5)
C8B	C19B	1.529(4)	C9D	C10D	1.412(5)
C9B	C10B	1.411(5)	C10D	C11D	1.383(5)
C10B	C11B	1.377(4)	C10D	C23D	1.531(5)
C11B	C12B	1.411(4)	C11D	C12D	1.406(4)
C13B	C14B	1.406(4)	C13D	C14D	1.403(4)
C13B	C18B	1.391(4)	C13D	C18D	1.396(4)
C14B	C15B	1.402(4)	C14D	C15D	1.400(4)
C15B	C16B	1.394(5)	C15D	C16D	1.393(4)
C15B	C27B	1.537(5)	C15D	C27D	1.541(4)
C16B	C17B	1.400(5)	C16D	C17D	1.390(4)
C17B	C18B	1.391(5)	C17D	C18D	1.394(4)

Table S5. Energies of the complexes calculated at CAM-B3LYP/DKH-def2-TZVP level.

Complex	Temperature	Ion	In Hartree atomic units			In cm^{-1}
			E_{LS}	E_{HS}	$E_{LS} - E_{HS}$	$E_{LS} - E_{HS}$
1	High	Fe1	–4438.955731	–4438.924726	–0.031005	–6804.80
2	High	Fe1A	–4436.512913	–4436.557350	0.044437	9752.76
2	High	Fe1B	–4436.520471	–4436.558130	0.037659	8265.12
2	Low	Fe1A	–4436.492469	–4436.529037	0.036569	8025.88
2	Low	Fe1B	–4436.513513	–4436.548245	0.034732	7622.90
2	Low	Fe1C	–4436.508080	–4436.556009	0.047929	10519.19
2	Low	Fe1D	–4436.543020	–4436.542700	–0.000321	–70.39

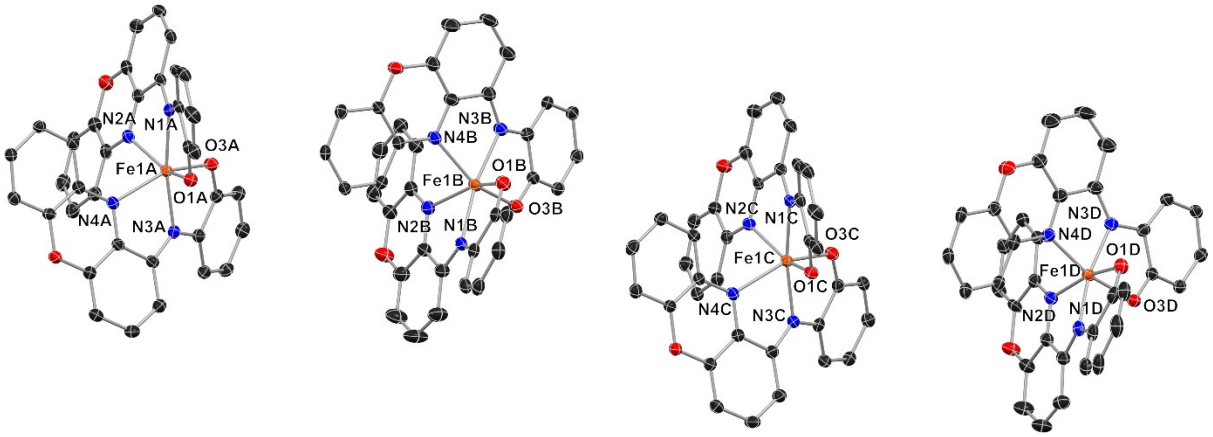

Figure S1 Illustration of the asymmetric unit of structure of **2** measured at 95 K. H atoms and *tert*-butyl groups are omitted for clarity.

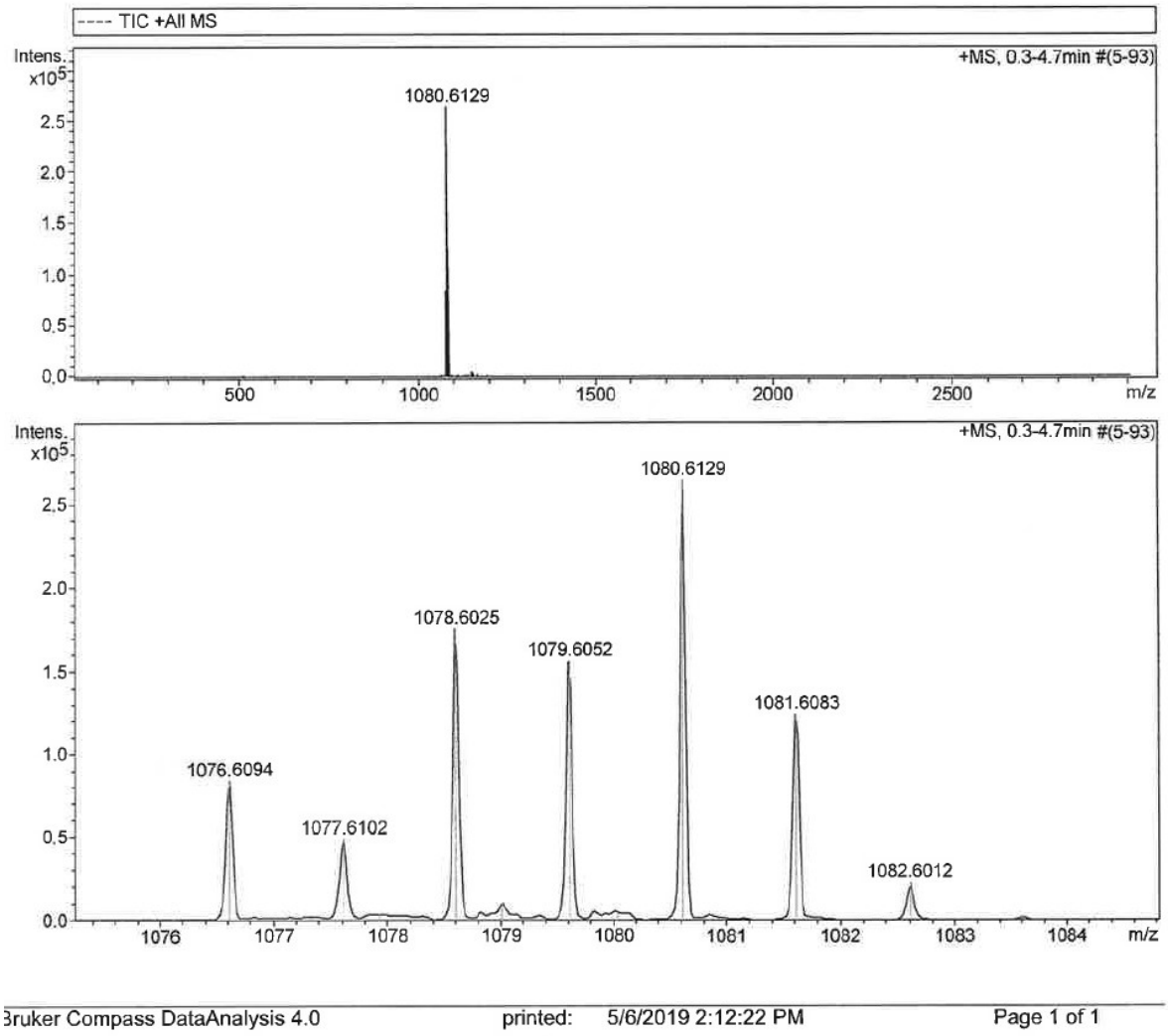

Figure S2 ESI-MS(+) spectrum of **2** in CH_2Cl_2

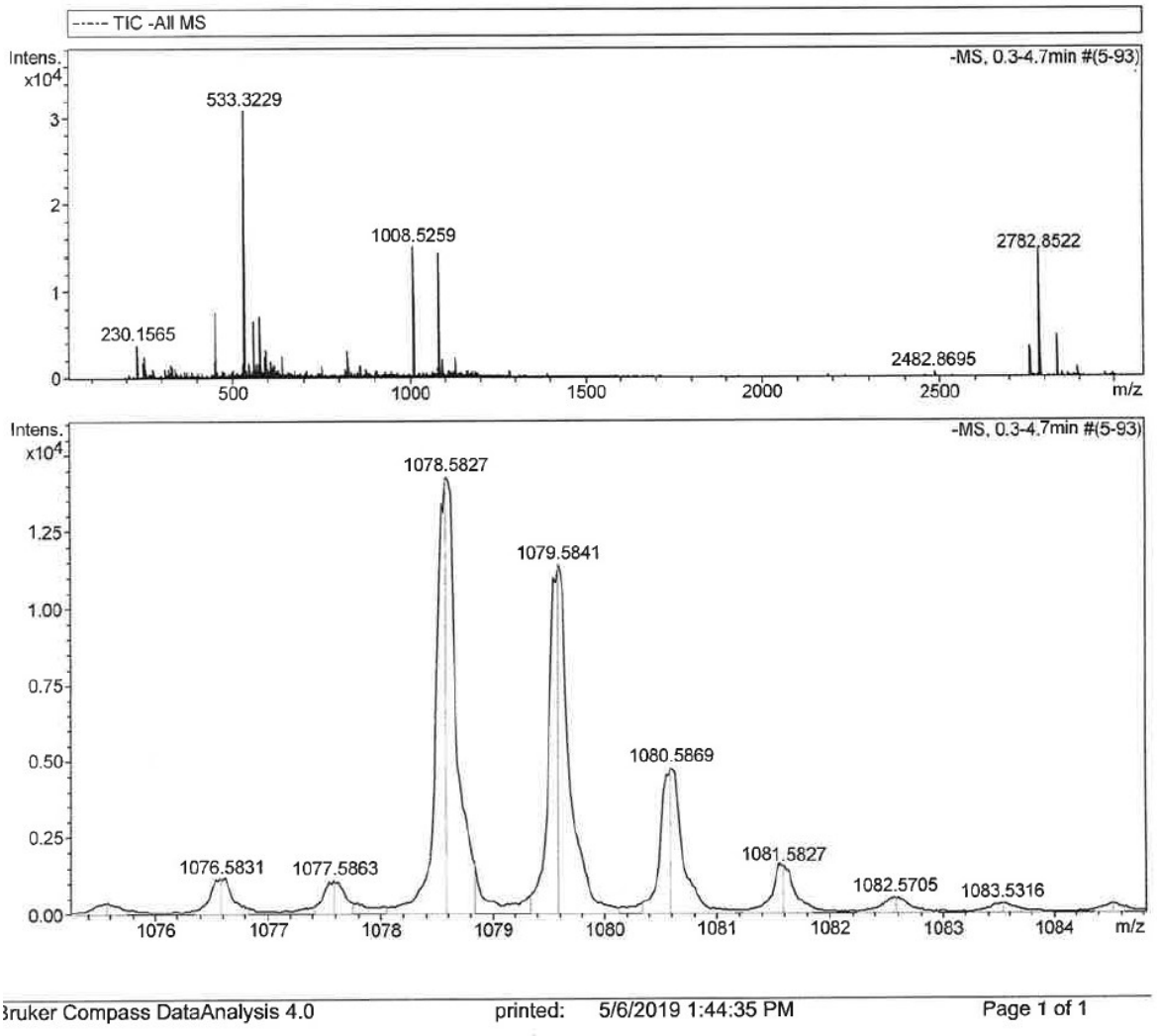

Figure S3 ESI-MS(-) spectrum of **2** in MeCN

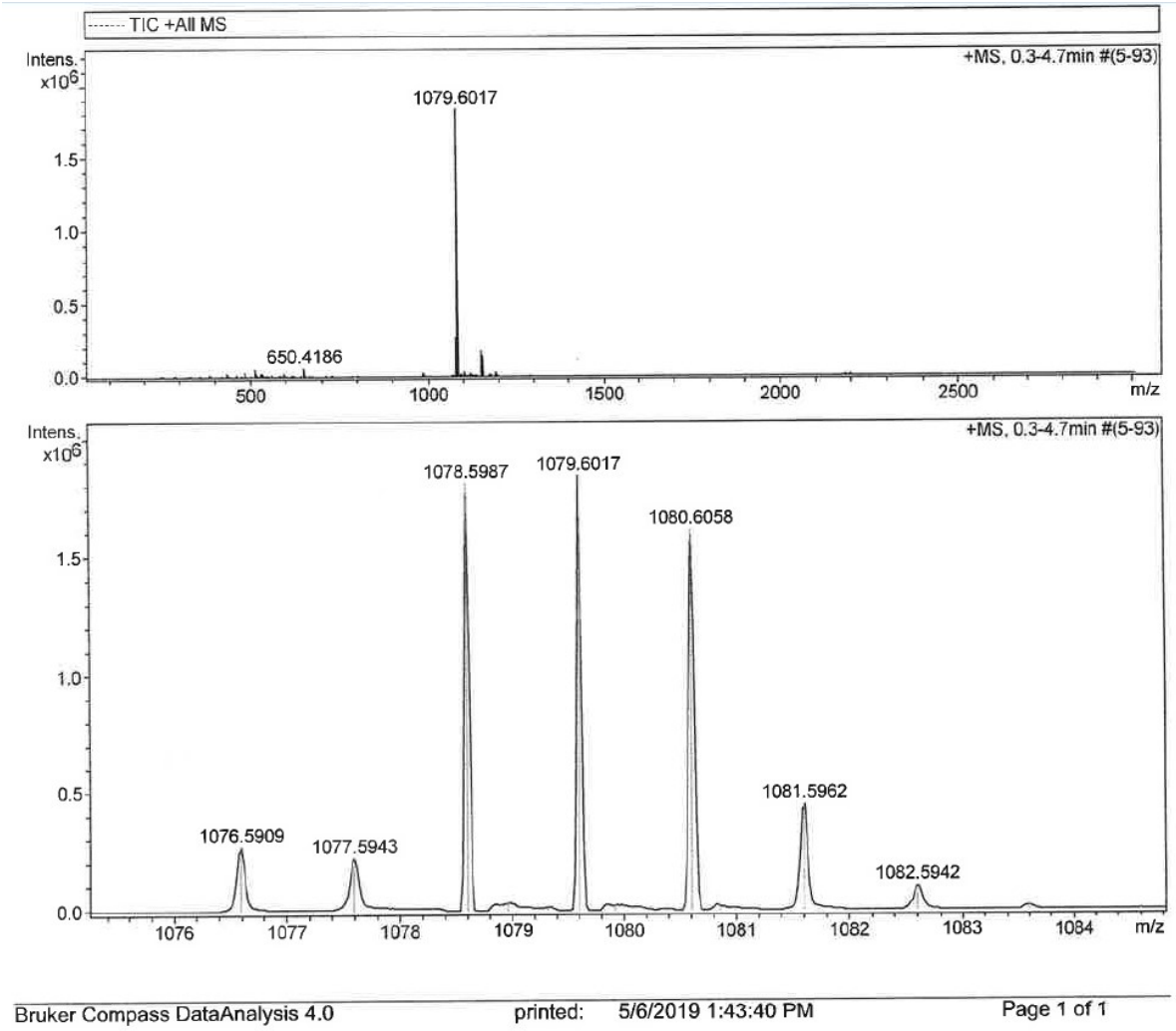

Figure S4 ESI-MS(+) spectrum of **2** in MeCN

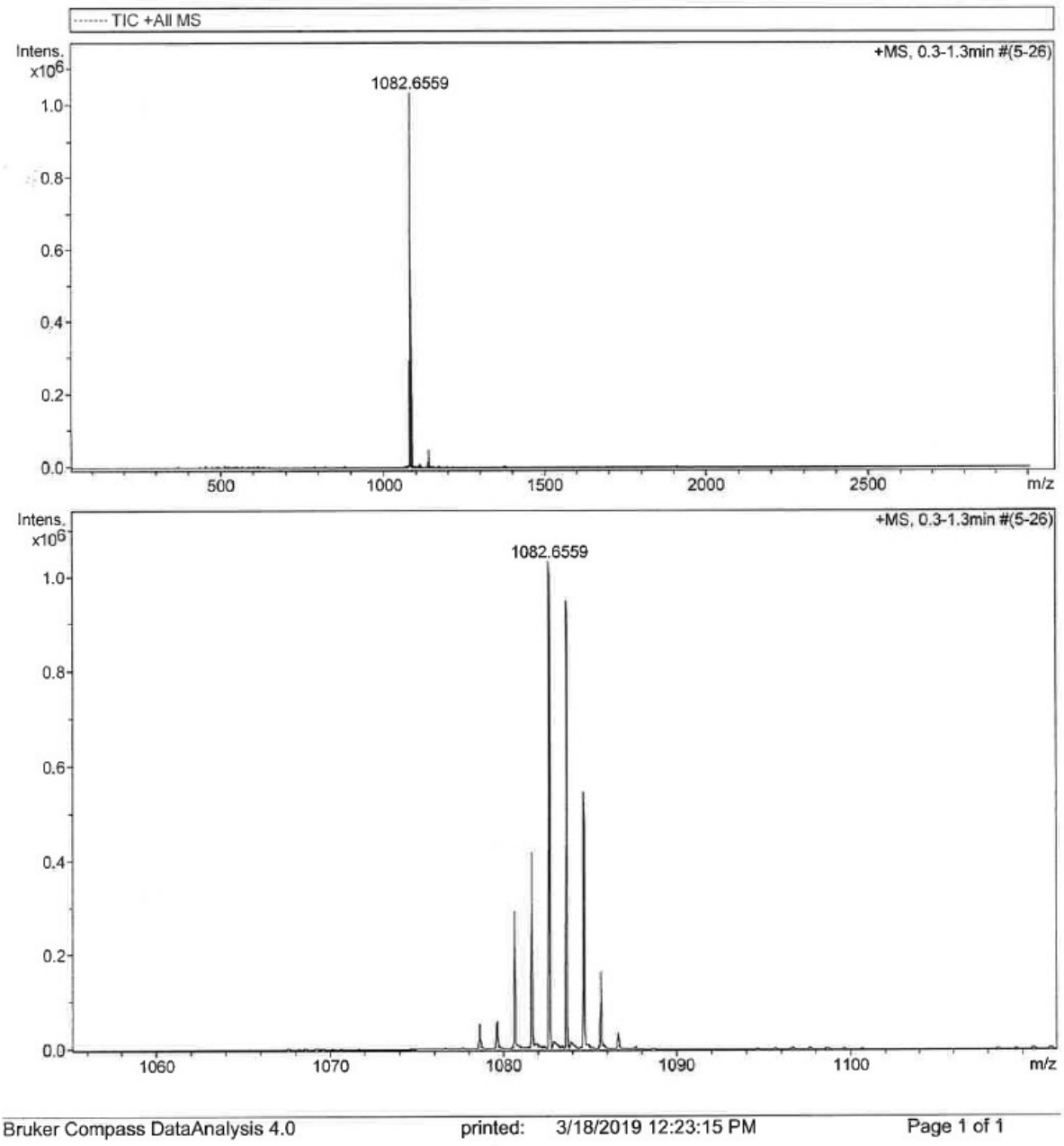

Figure S5 ESI-MS(+) spectrum of **1** in CH_2Cl_2

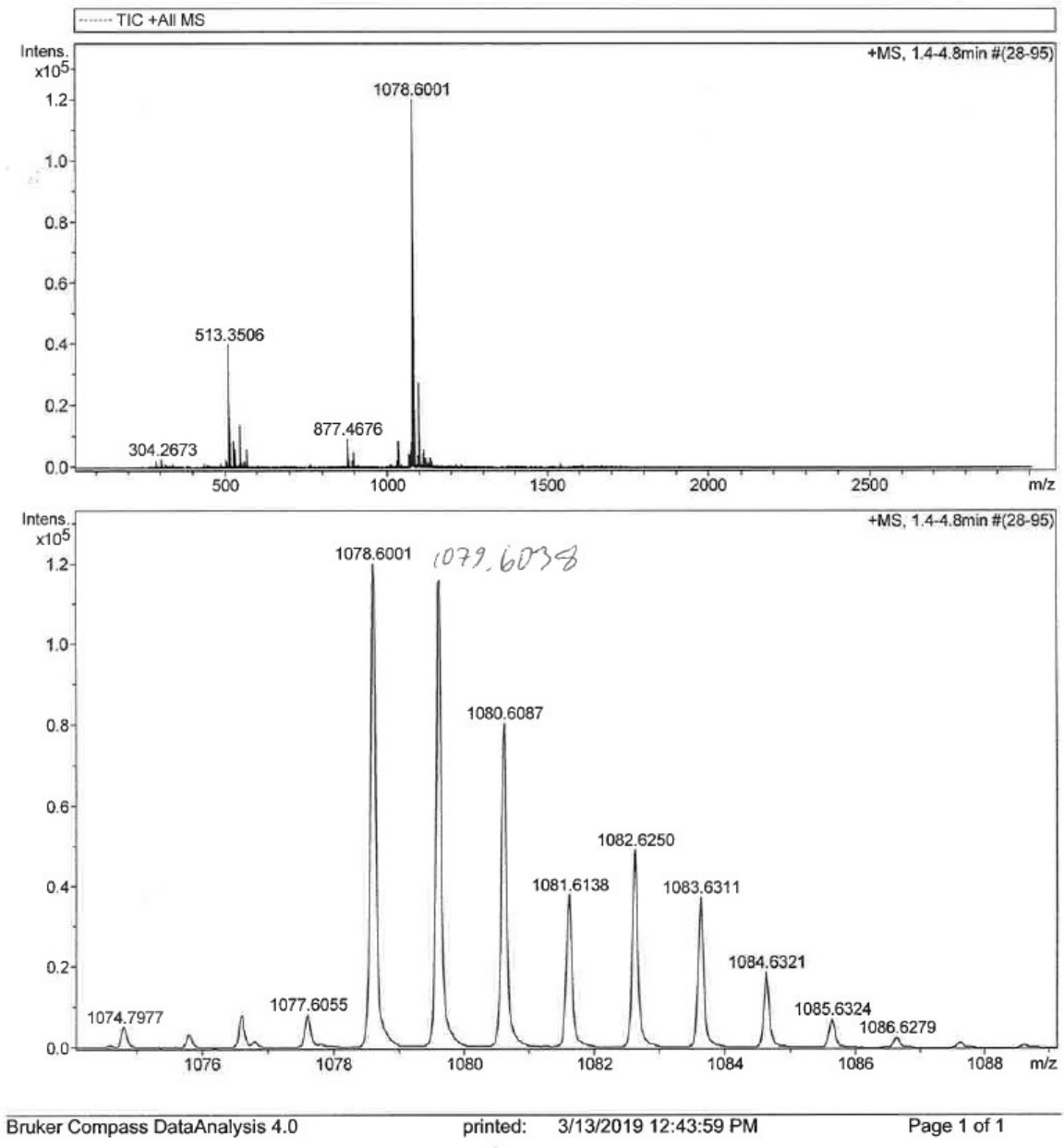

Figure S6 ESI-MS(+) spectrum of **1** in MeCN

Cyclic voltammetry (CV) was applied to define the redox stabilities and the characteristic redox behaviour of the complexes, while the voltammograms were measured in the potential range from +1.5 to –2.1 V vs. Fc^+/Fc.[18] During the first three or four scans, the voltammograms underwent an alteration process for both complexes. During these processes, some of the signals were lost from the voltammograms and then the signals that were left, stayed for subsequent scans. CV for **1** and **2** were recorded at ambient temperature using a platinum working electrode, a 1-mm-diameter platinum counter electrode, and a Ag/AgCl reference electrode. Samples were dissolved in CH_2Cl_2 containing 0.1 M $(Bu_4N)ClO_4$ as the supporting electrolyte. The voltammogram was recorded at scan rate of 100 mV/s, while the potentials were measured in volts versus the Fc+/Fc couple. The continuous scanning of **1** produced two, reversible one-electron transfer waves at -0.21 and +0.61 V. For **2**, the voltammogram manifested two observable one-electron transfer waves at -0.12 and +0.52 V.

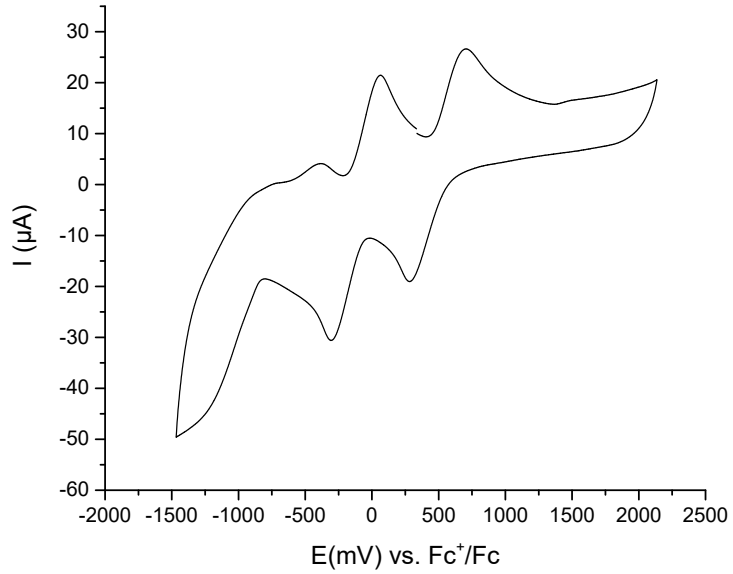

Figure S7 CV for **2** measured in CH_2Cl_2 potential vs. Fc^+/Fc at 300 mVs^{-1} scan rate at RT. The scan is performed in a clockwise manner.

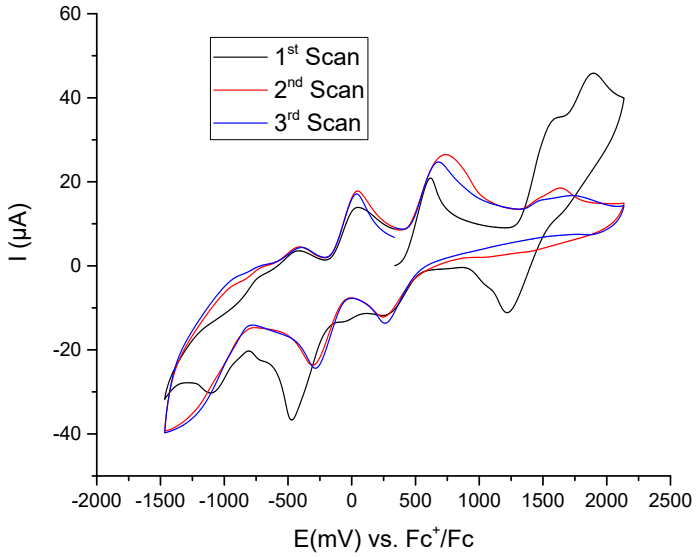

Figure S8 The first CV scans for **2** measured in CH_2Cl_2 potential vs. Fc^+/Fc at 200 mVs^{-1} scan rate at RT. The scan is performed in a clockwise manner.

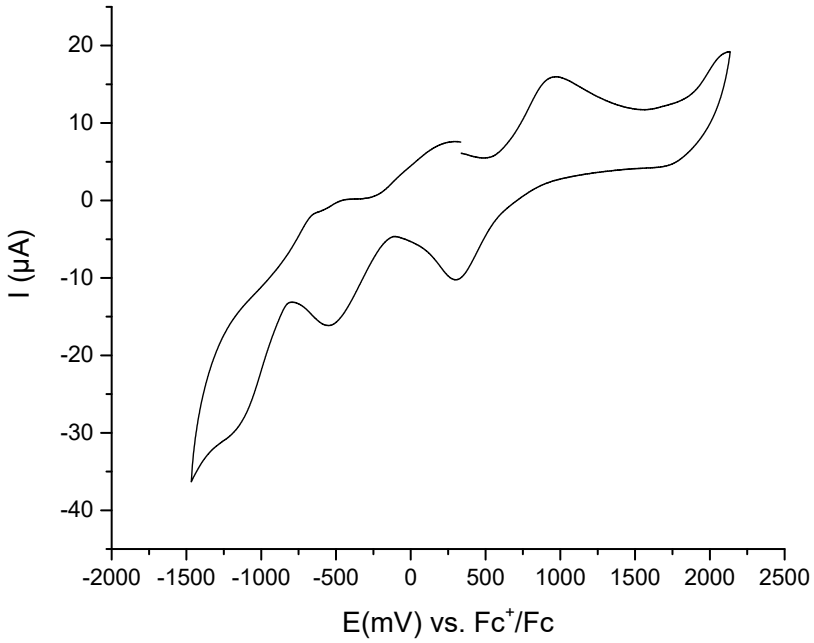

Figure S9 CV for **1** measured in CH_2Cl_2 potential vs. Fc^+/Fc at 300 mVs^{-1} scan rate at RT. The scan is performed in a clockwise manner.

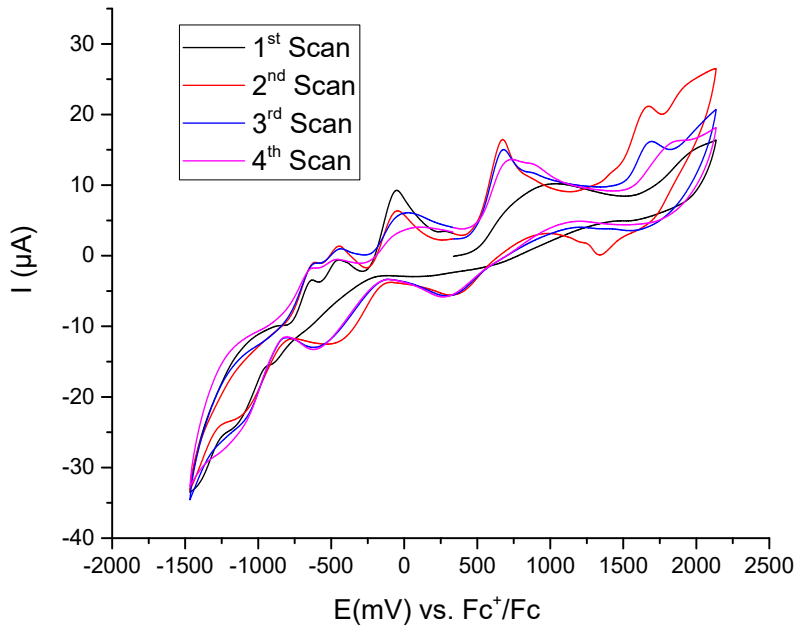

Figure S10 The first CV scans for **1** measured in CH_2Cl_2 potential vs. Fc^+/Fc at 200 mVs^{-1} scan rate at RT. The scan is performed in a clockwise manner.

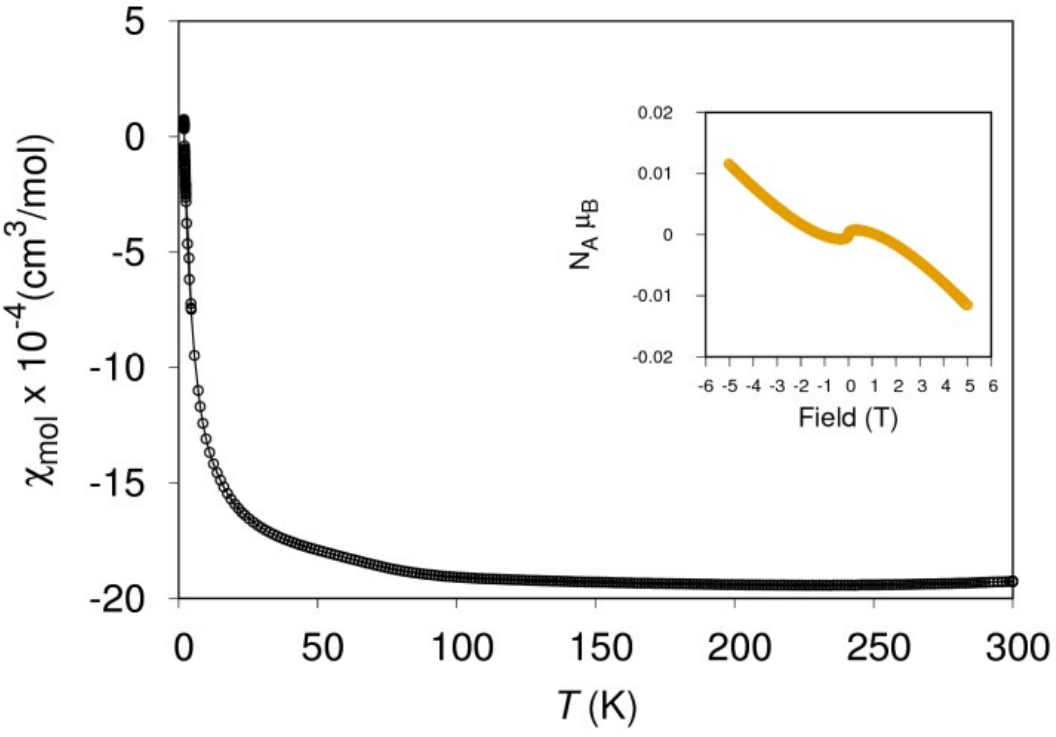

Figure S11 SQUID measurements for **1** measured in the solid state. The inset represents the field dependence at 2K for **1**.

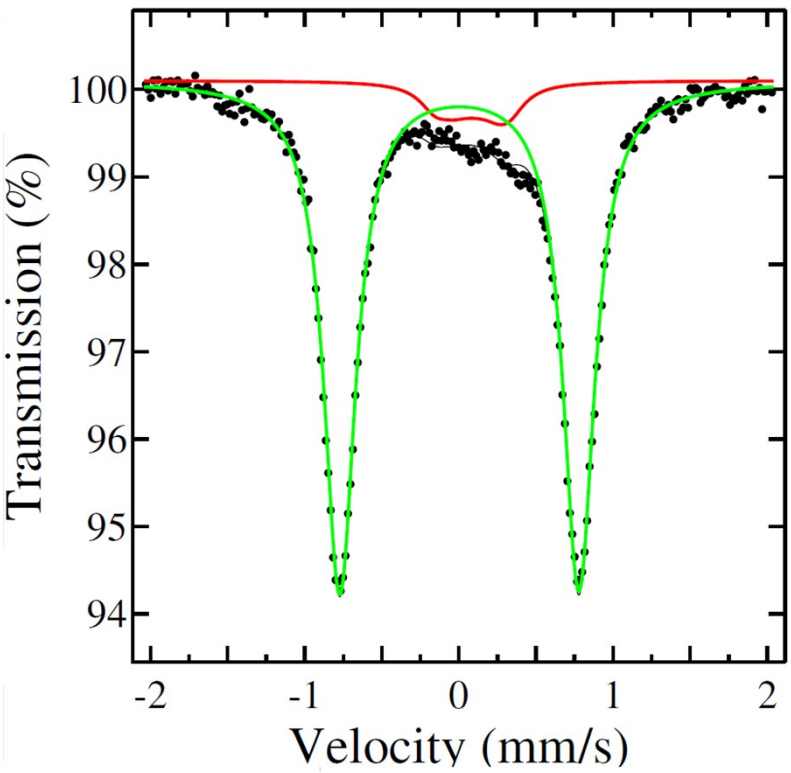

Figure S12 Mössbauer measurements for **1** measured at 77 K. The red signal is Fe impurity present in the apparatus.

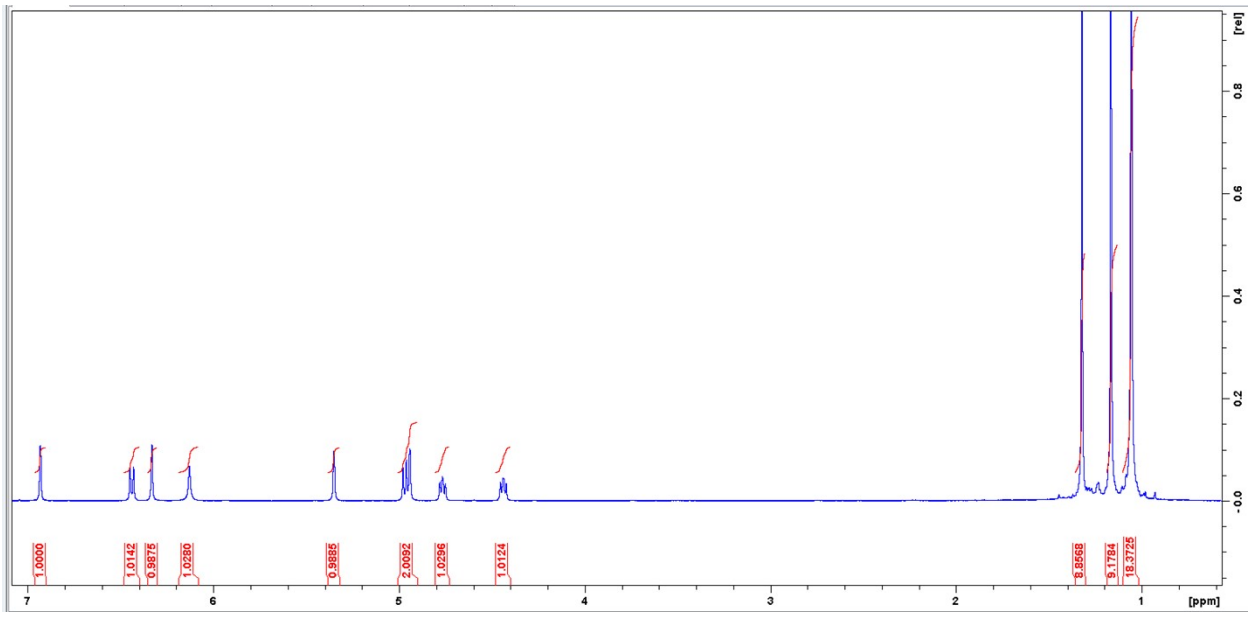

Figure S13 Measured ^{1}H-NMR spectrum for **1**

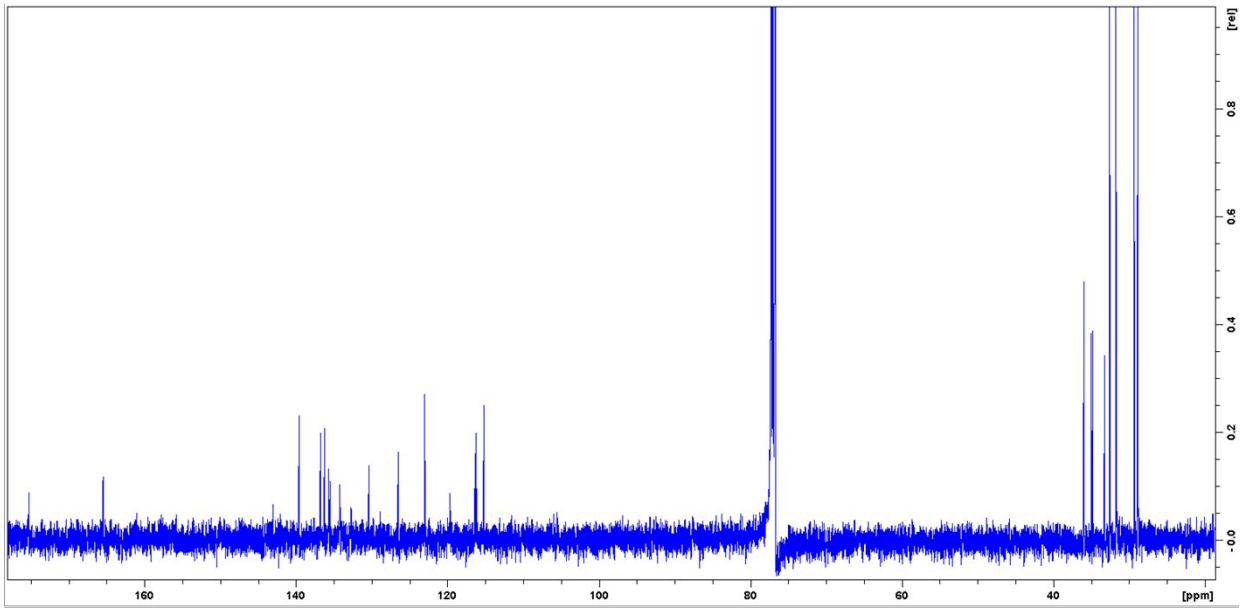

Figure S14 Measured ^{13}C-NMR spectrum for **1**

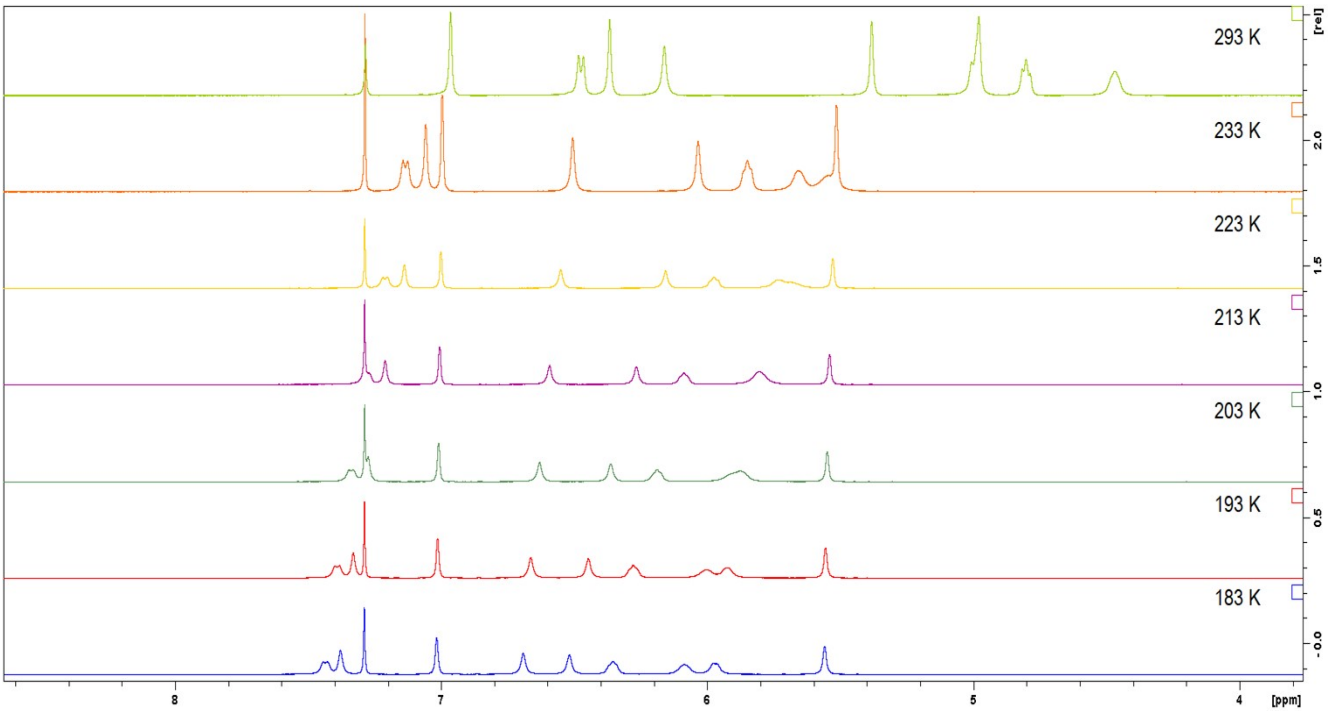

Figure S15 The aromatic area of the measured ^{1}H-NMR spectrum for **1** at variable temperatures

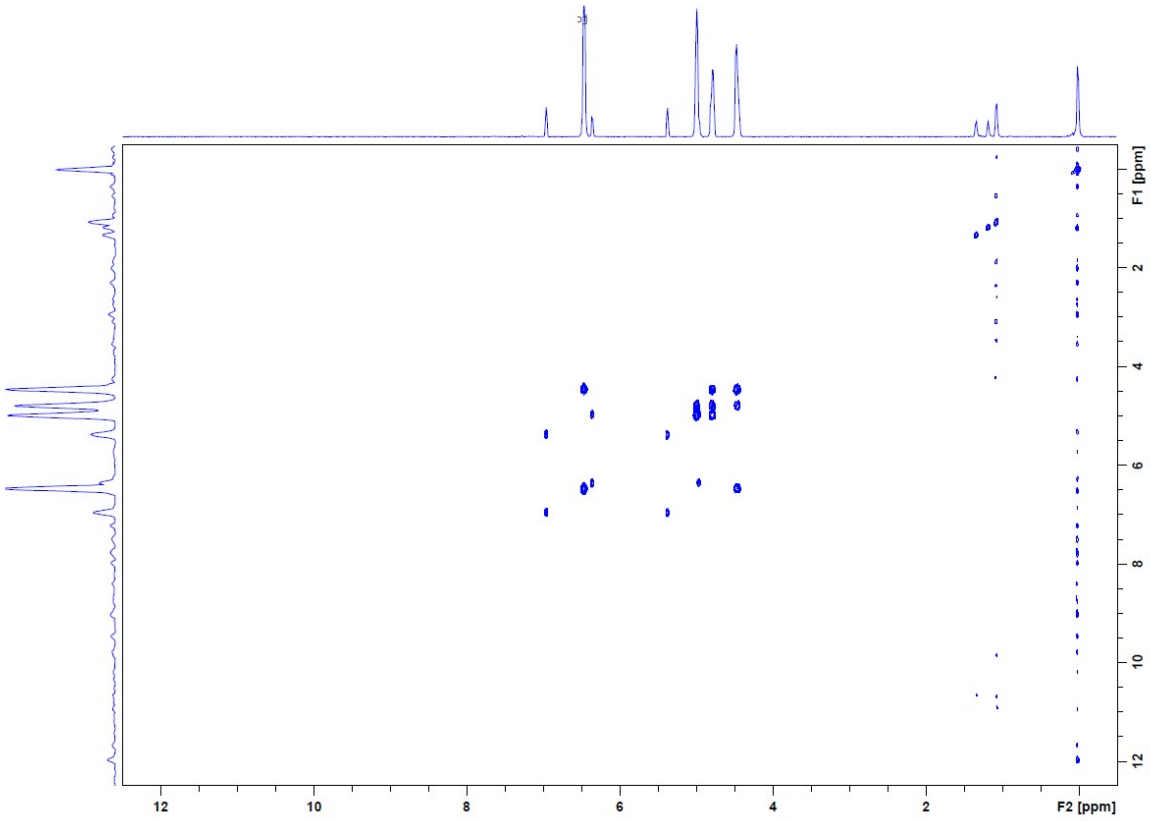

Figure S16 The 2D-COSY spectrum for **1**.

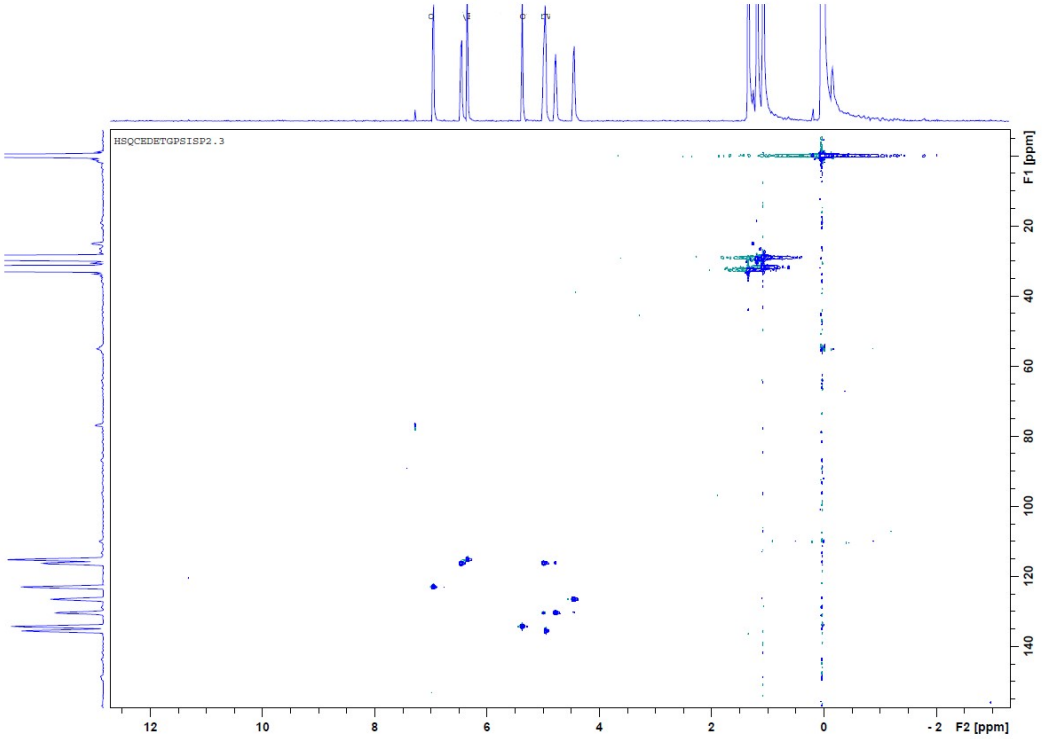

Figure S17 The 2D-HSQC spectrum for **1**.

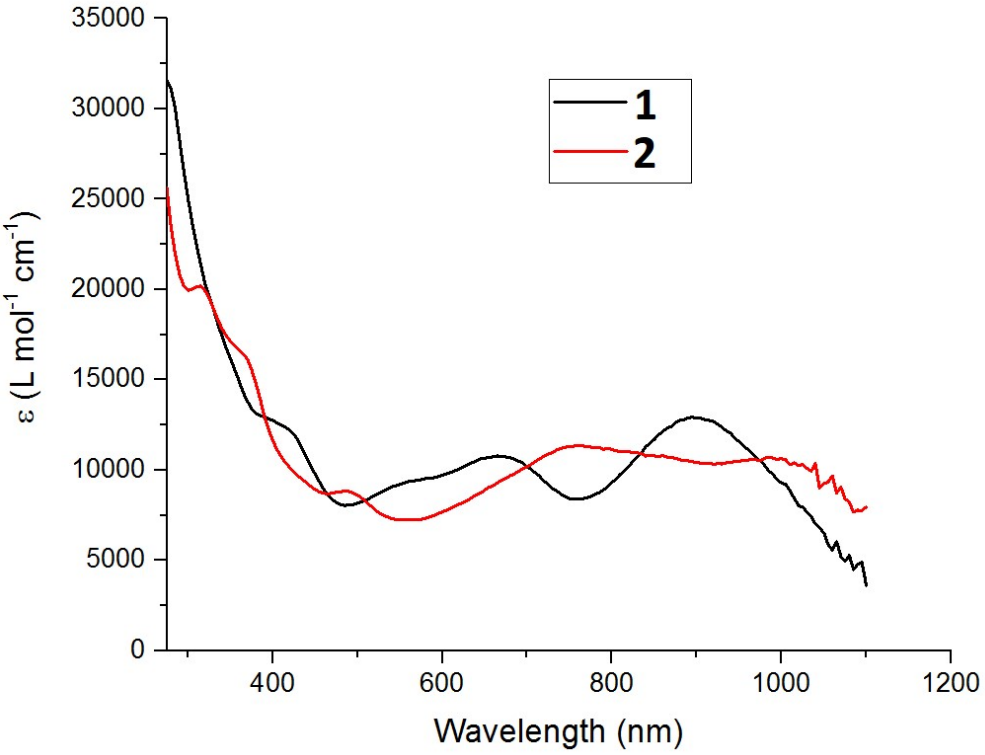

Figure S18 UV/vis/NIR spectra of the iron complexes in CH_2Cl_2 solution at RT.

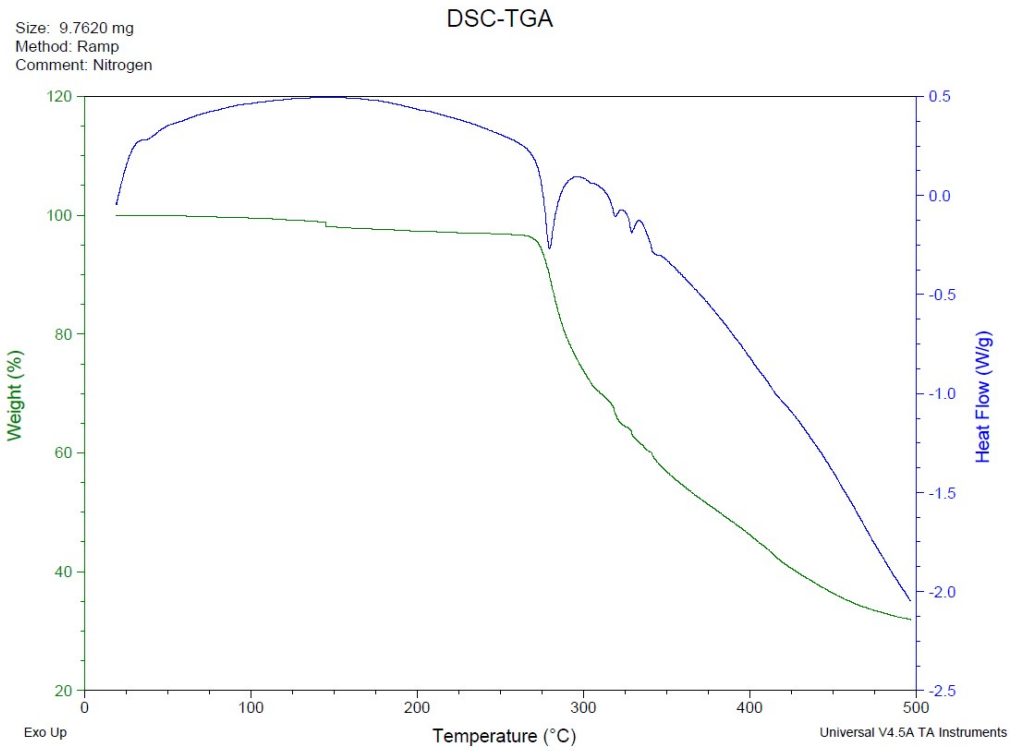

Figure S19 TGA-DSC measurements for **1**.

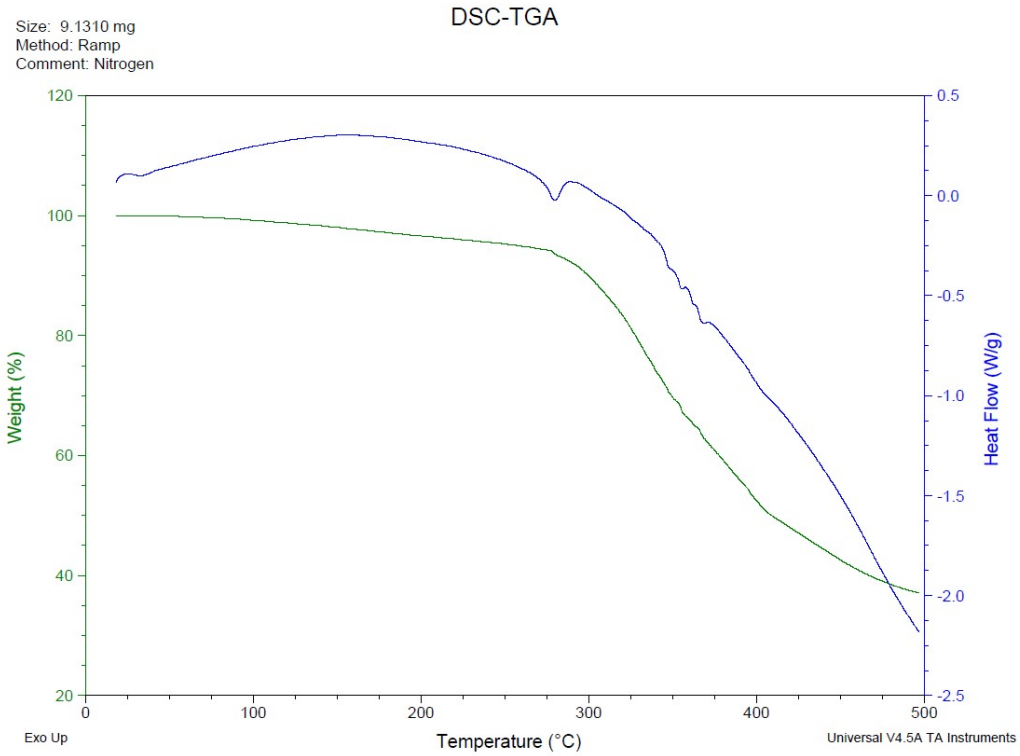

Figure S20 TGA-DSC measurements for **2**.

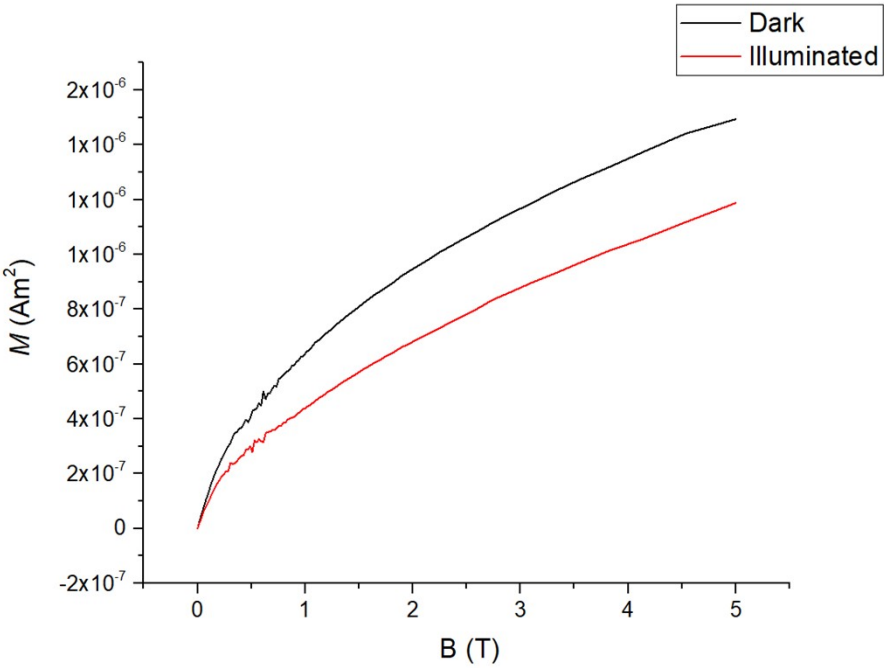

Figure S21 The measured virgin curves of **1** on a $SrTiO_3$ disk at 2 K.

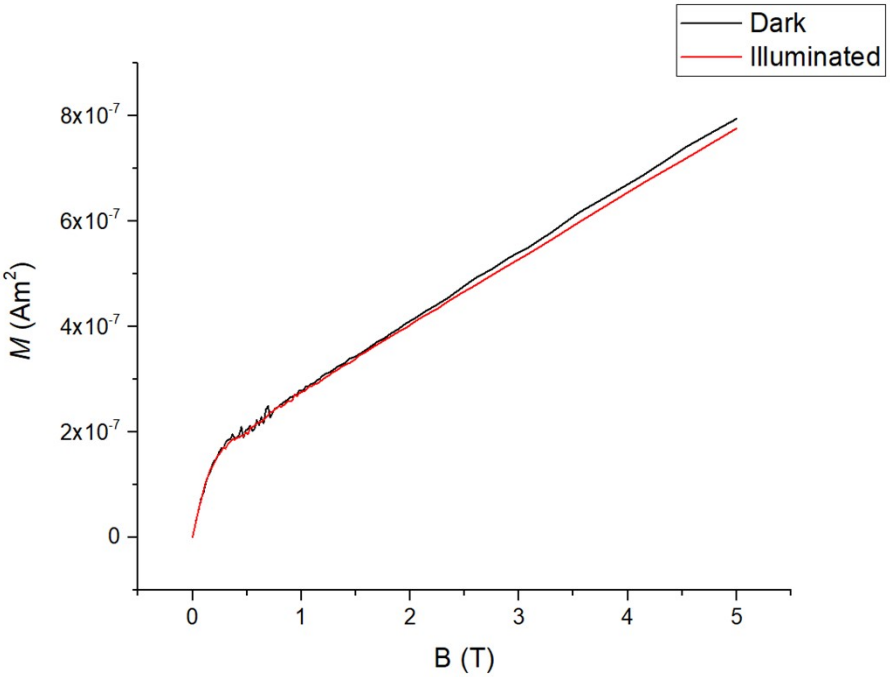

Figure S22 The measured virgin curves of **1** on a $SrTiO_3$ disk at 30 K.

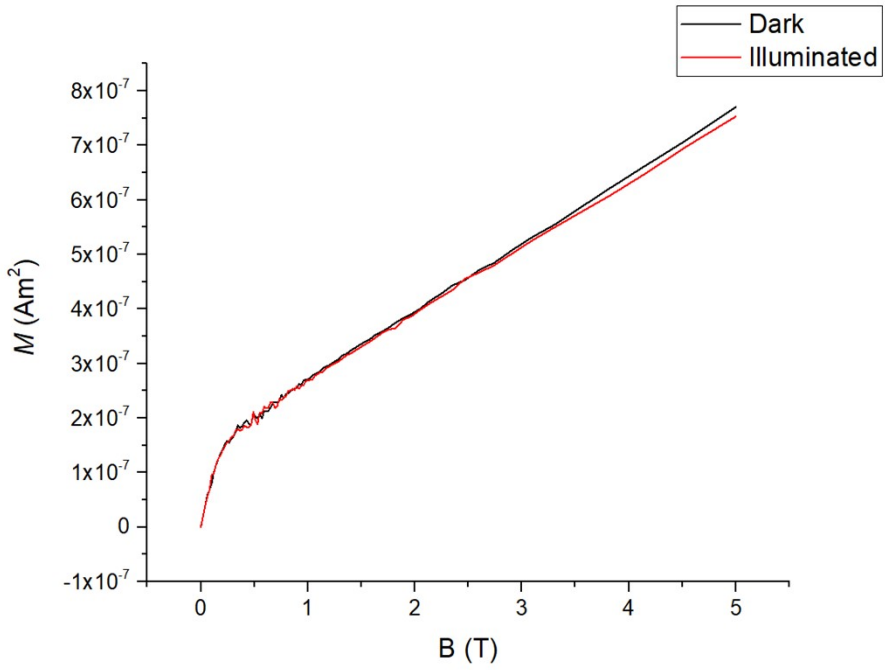

Figure S23 The measured virgin curves of **1** on a $SrTiO_3$ disk at 50 K.

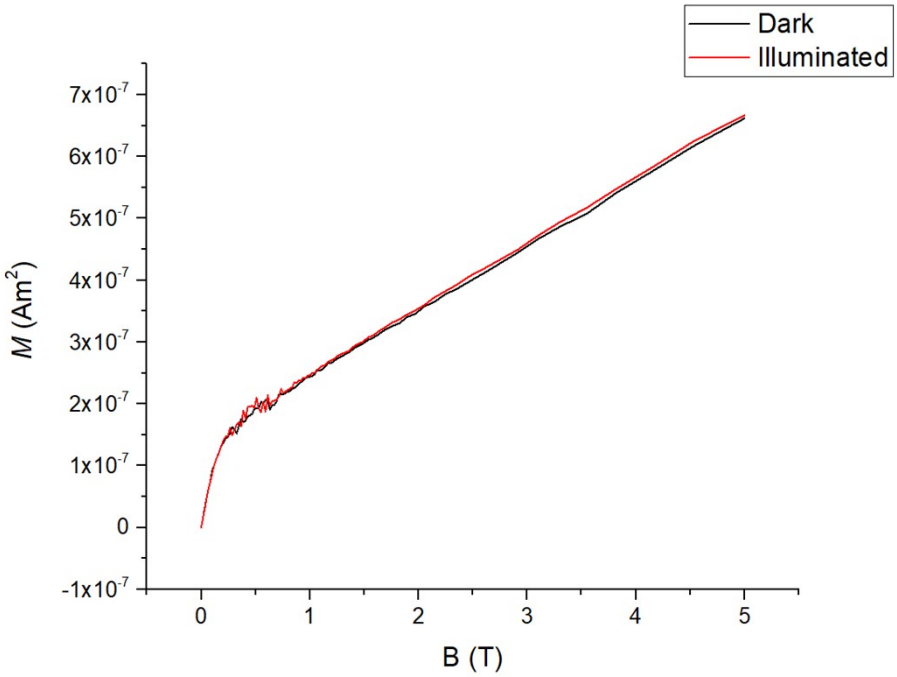

Figure S24 The measured virgin curves of **1** on a $SrTiO_3$ disk at 100 K.

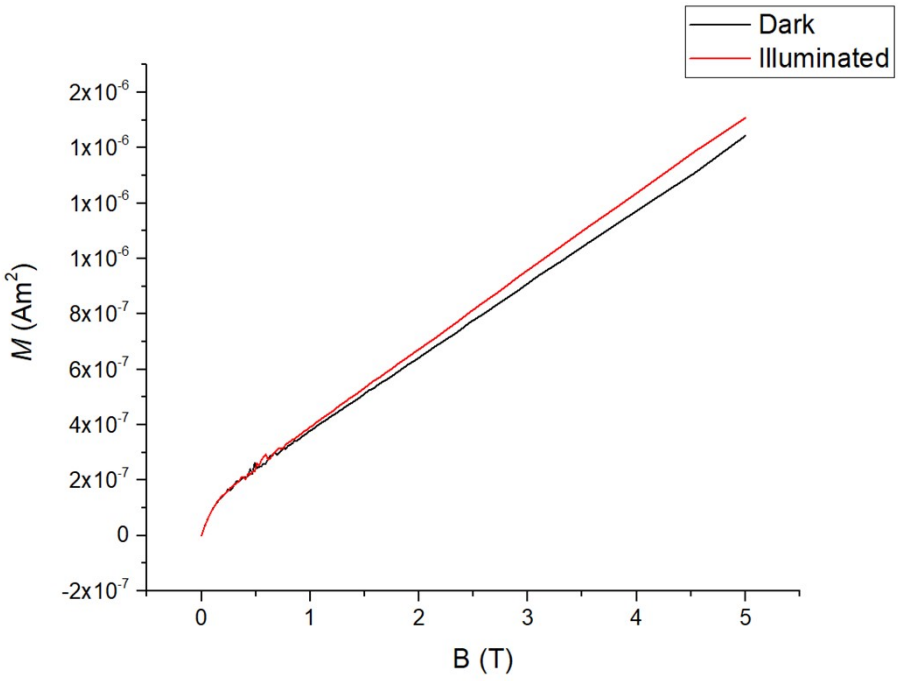

Figure S25 The measured virgin curves of **1** on a $SrTiO_3$ disk at 300 K.

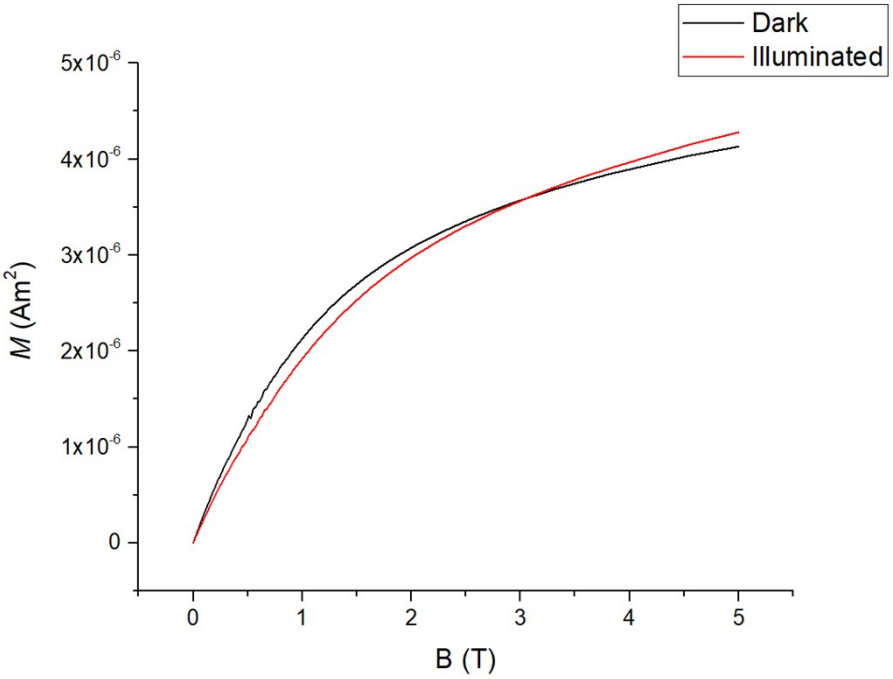

Figure S26 The measured virgin curves of **2** on a $SrTiO_3$ disk at 2 K.

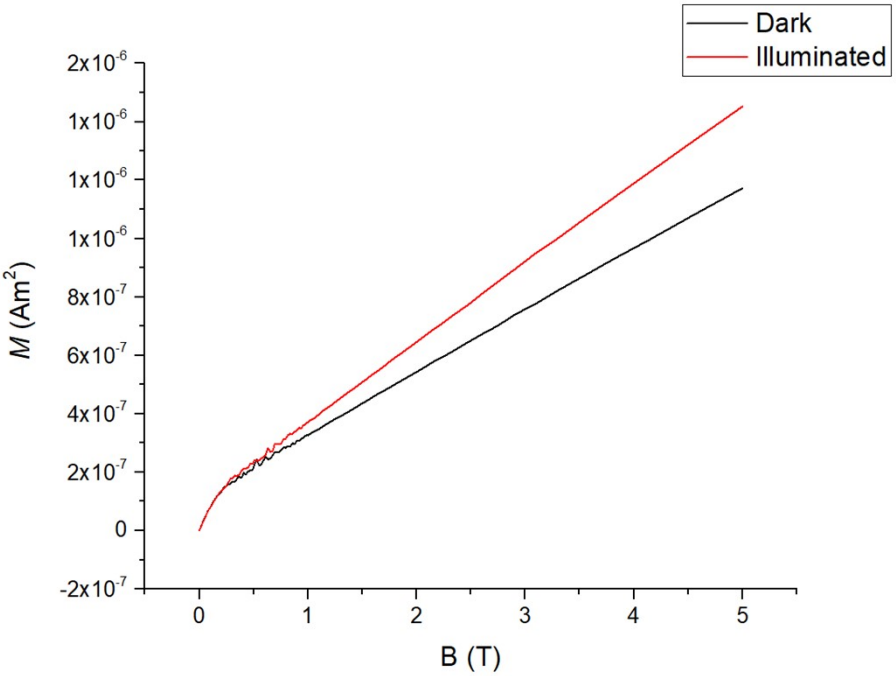

Figure S27 The measured virgin curves of **2** on a $SrTiO_3$ disk at 30 K.

Figure S28 The measured virgin curves of **2** on a $SrTiO_3$ disk at 50 K.

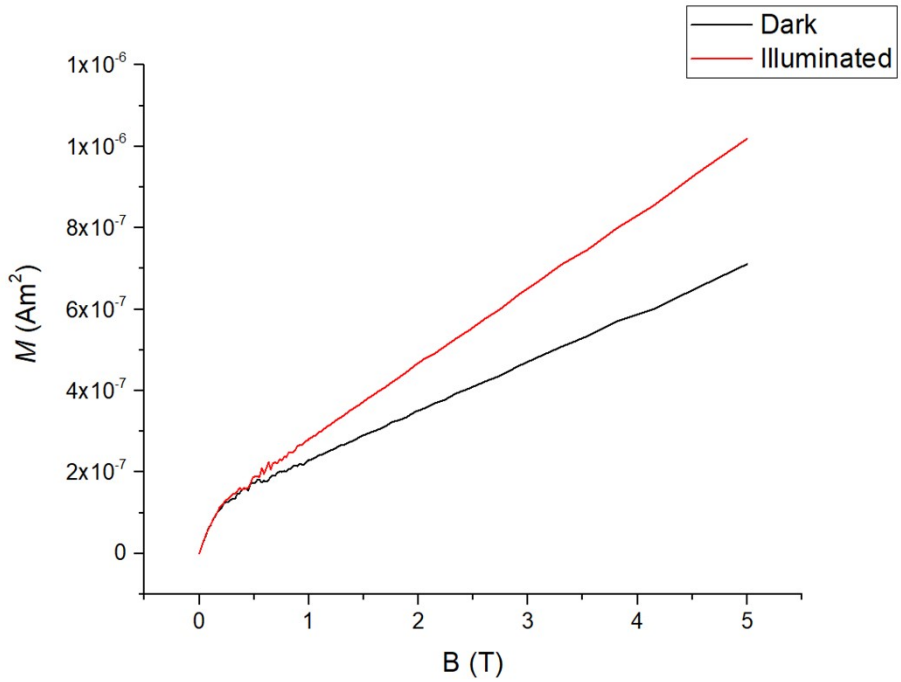

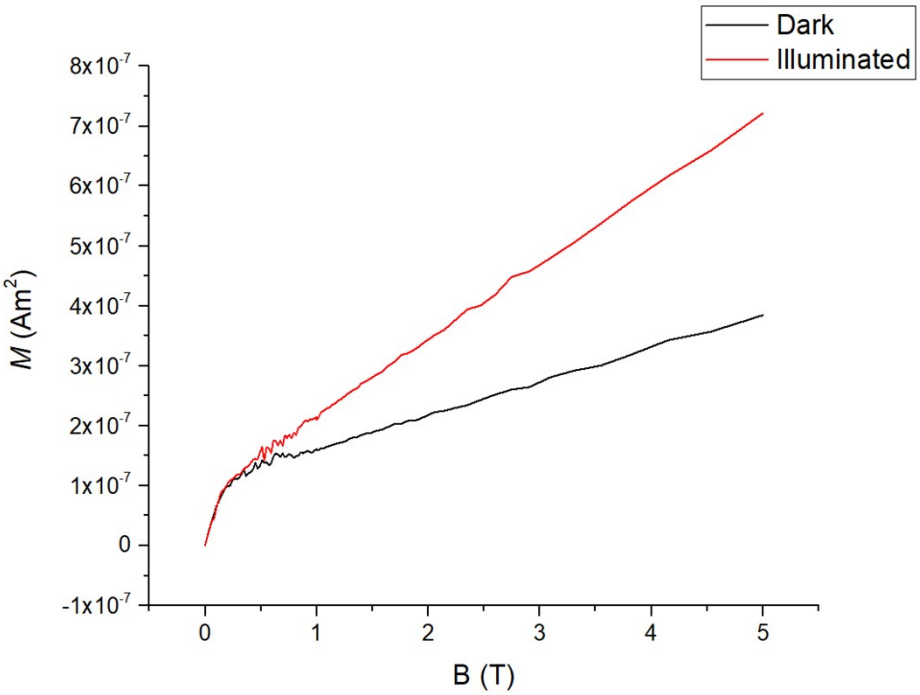

Figure S29 The measured virgin curves of **2** on a $SrTiO_3$ disk at 100 K.

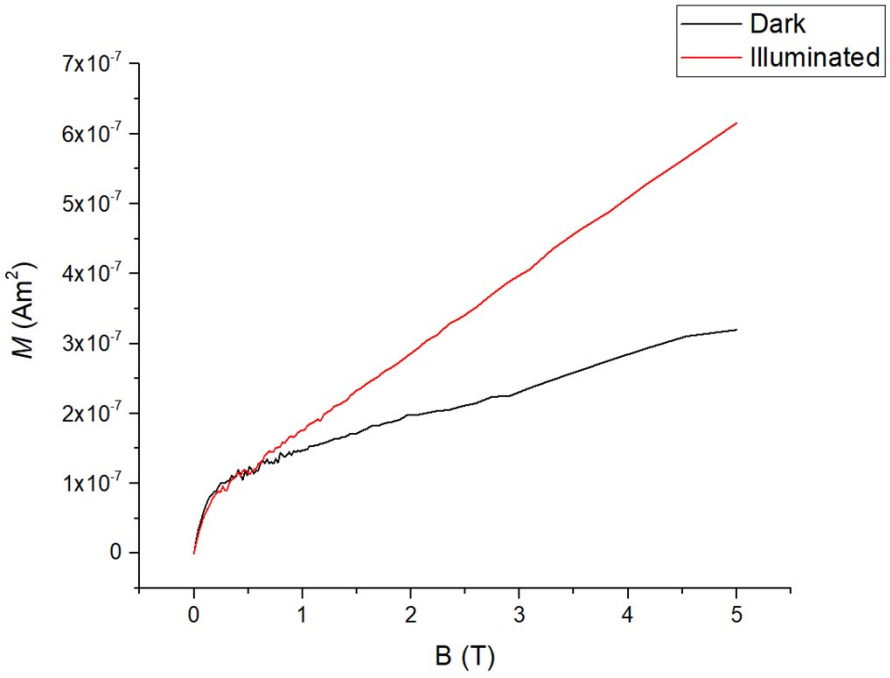

Figure S30 The measured virgin curves of **2** on a $SrTiO_3$ disk at 300 K.

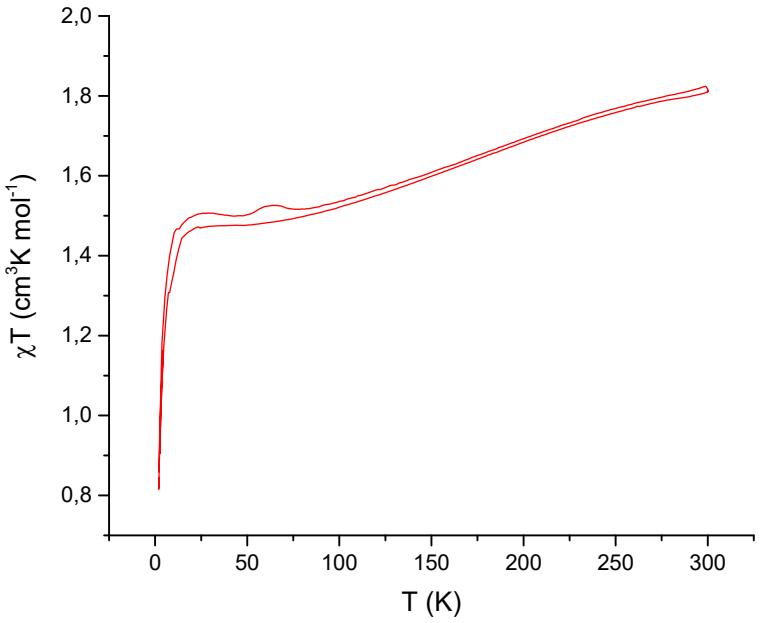

Figure S31 SQUID variable temperature measurements for **2** measured from the amorphous solid at 1 T magnetic field.

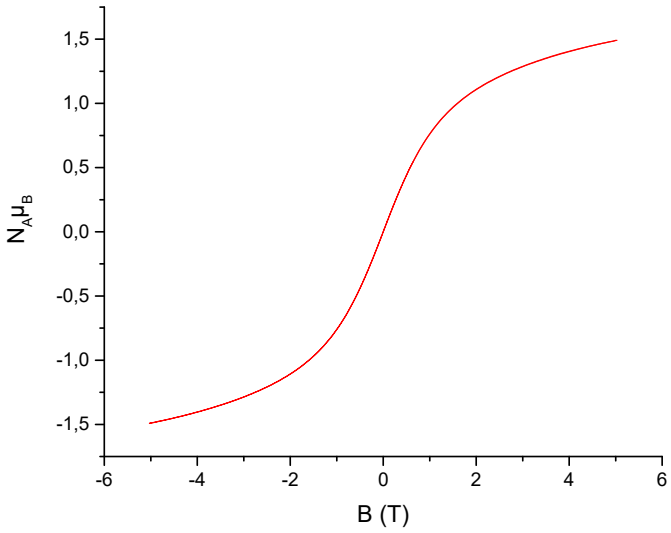

Figure S32 SQUID variable magnetic field measurements for **2** measured from the amorphous solid at 2 K temperature.

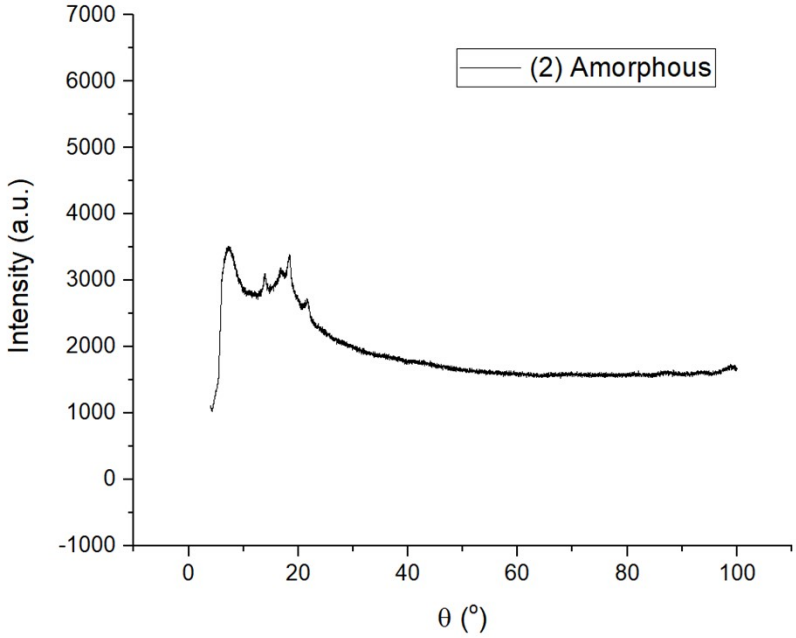

Figure S33 Powder X-ray diffraction pattern of the amorphous sample of **2** at RT.

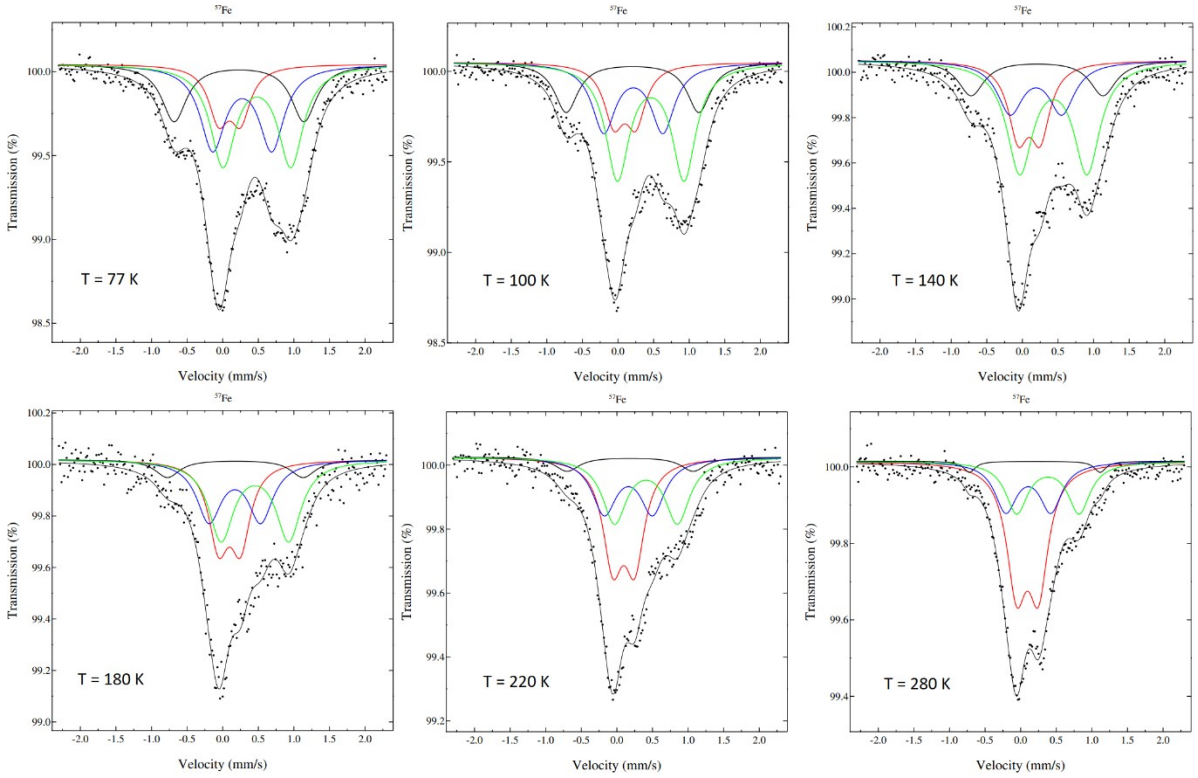

Figure S34 Variable temperature Mössbauer spectra of the amorphous sample of **2**. The red signal is due to an instrumental impurity.

References

(1) Blackmore, K. J.; Lal, N.; Ziller, J. W.; Heyduk, A. F. *Eur. J. Inorg. Chem.* **2009**, No. 6, 735–743.

(2) Chaudhuri, P.; Hess, M.; Müller, J.; Hildenbrand, K.; Bill, E.; Weyhermüller, T.; Wieghardt, K. *J. Am. Chem. Soc.* **1999**, *121* (41), 9599–9610.

(3) CrysAlisPro program; version 1.171.38.43; Rigaku Oxford Diffraction: Oxford 2015.

(4) Sheldrick, G. M. *Acta Crystallogr. Sect. A Found. Crystallogr.* **2007**, *64*, 112–122.

(5) Sheldrick, G. M. *Acta Crystallogr. Sect. C Struct. Chem.* **2015**, *71* (Md), 3–8.

(6) Dolomanov, O. V.; Bourhis, L. J.; Gildea, R. J.; Howard, J. A. K.; Puschmann, H. *J. Appl. Crystallogr.* **2009**, *42* (2), 339–341.

(7) F. Neese. *WIREs Comput. Mol. Sci.* **2017**, *8*, e1327.

(8) F. Neese, F. Wennmohs, U. Becker, C. Riplinger. *J. Chem. Phys.* **2020**, *152*, 224108.

(9) J. P. Perdew, K. Burke, M. Ernzerhof. *Phys. Rev. Lett.*, **1996**, *77*, 3865–3868.

(10) J. P. Perdew, K. Burke, M. Ernzerhof. *Phys. Rev. Lett.*, **1996**, *78*, 1396.

(11) T. Yanai, D. P. Tew, N. C. Handy. *Chem. Phys. Lett.* **2004**, *393*, 51–57.

(12) A. D. Becke. *Phys. Rev. A.* **1988**, *38*, 3098–3100.

(13) C. Lee, W. Yang, R. G. Parr. *Phys. Rev. B.* **1988**, *37*, 785–789.

(14) M. Douglas, N. M. Kroll. *Ann. Phys.* **1974**, *82*, 89–155.

(15) B. A. Heß. *Phys. Rev. A.* **1986**, *33*, 3742–3748.

(16) D. A. Pantazis, X.-Y. Chen, C. R. Landis, F. Neese. *J. Chem. Theory Comput.* **2008**, *4*, 908–919.

(17) F. Weigend, R. Ahlrichs. *Phys. Chem. Chem. Phys.* **2005**, *7*, 3297–3305.

(18) R. R. Gagne, C. A. Koval and G. C. Lisensky, *Inorg. Chem.*, 1980, **19**, 2854–2855.